Biosensors and Bioelectronics 200 (2022) 113926

Contents lists available at ScienceDirect

Biosensors and Bioelectronics

journal homepage: www.elsevier.com/locate/bios

Enhancing the electrocatalytic activity of palladium nanocluster tags by selective introduction of gold atoms: Application for a wound infection biomarker detection

Celia Toyos-Rodríguez [a,b], Alaa Adawy [c], Francisco Javier García-Alonso [b,d], Alfredo de la Escosura-Muñiz [a,b,*]

[a] NanoBioAnalysis Group-Department of Physical and Analytical Chemistry, University of Oviedo, Julián Clavería 8, 33006, Oviedo, Spain
[b] Biotechnology Institute of Asturias, University of Oviedo, Santiago Gascon Building, 33006, Oviedo, Spain
[c] Unit of Electron Microscopy and Nanotechnology, Institute for Scientific and Technological Resources (SCTs), Edificio Severo Ochoa S/n, Campus de El Cristo, 33006, Oviedo, Spain
[d] NanoBioAnalysis Group-Department of Organic and Inorganic Chemistry, University of Oviedo, Julián Clavería 8, 33006, Oviedo, Spain

ARTICLE INFO

Keywords:
Palladium nanocluster
Electrocatalysis
Bimetallic nanoparticles
Immunosensor
Wound infection
Biomarker

ABSTRACT

In this work, an unprecedented study exploring the role that slight changes into the Pd/Au proportion have in the electrocatalytic activity of bimetallic Pd-AuNPs toward the oxygen reduction reaction (ORR) is conducted. In particular, a careful control of the amount of Au atoms introduced in the cluster and the evaluation of the optimum Pd:Au ratio for getting the maximum catalytic activity is performed for the first time.

First, PdNPs are synthesized by alcohol reduction in the presence of polyvinylpyrrolidone, and gold atoms are selectively introduced on vertex or corner positions of the cluster in different amounts following a galvanic substitution procedure. Average elemental analysis done relying on EDX spectroscopy allows to evaluate the Pd:Au ratio in the Pd-AuNPs obtained. Lineal sweep voltammetry and chronoamperometry are used for the evaluation of the Pd-AuNPs electrocatalytic activity toward ORR at a neutral pH compared to PdNPs and AuNPs alone. Our results indicate that, the synergy between both metals is strongly enhanced when the amount of gold is controlled and occupies the more reactive positions of the cluster, reaching a maximum activity for the NPs containing a 30% of gold, while an excess of this metal leads to a decrease in such activity, as a shelter of the PdNPs is achieved. Chronoamperometric analysis allows the quantification of the optimal Pd-AuNPs at over 6×10^9 NPs/mL levels.

Such optimal Pd-AuNPs were used as tags, taking advantage of the bio-functionalities of gold present in the cluster, in a proof-of-concept electrochemical immunosensor for the detection of hyaluronidase wound infection biomarker, using magnetic beads as platforms. Hyaluronidase was detected at levels as low as 50 ng/mL (0.02 U/mL; 437 U/mg) with good reproducibility (RSD below 8%) and selectivity (evaluated against bovine serum albumin, immunoglobulin G and lysozyme). The low matrix effects inherent to the use of magnetic bead platforms allowed us to discriminate between wound exudates with both sterile and infected ulcers without sample pretreatment. This novel electrocatalytic immunoassay has the advantage, over common methods for NP tags electrochemical detection, of the signal generation in the same neutral medium where the immunoassay takes place (10 mM PBS pH 7.4), avoiding the use of additional and hazardous reagents, bringing it closer to their use as point-of-care devices.

Overall, our findings may be of great interest not only for biosensing, but also for applications such as energy converting on fuel cells, in which the ORR has a pivotal role.

* Corresponding author. NanoBioAnalysis Group-Department of Physical and Analytical Chemistry, University of Oviedo, Julián Clavería 8, 33006, Oviedo, Spain.
E-mail address: alfredo.escosura@uniovi.es (A. de la Escosura-Muñiz).

https://doi.org/10.1016/j.bios.2021.113926
Received 25 October 2021; Received in revised form 11 December 2021; Accepted 25 December 2021
Available online 30 December 2021

1. Introduction

The use of nanomaterials has been a breakthrough since they were first synthesized and implemented into different research topics with continuous progress (Bayda et al., 2020; Welch and Compton, 2006). Biosensing is among the main areas of application of these materials, in which the usage of nanomaterials, both as electrode modifiers and as labels has implied a significant improvement. Their unique properties, including electron transfer, biocompatibility and electroactive and electrocatalytic activity, among others, has enabled decreasing detection limits and increasing sensitivity, selectivity and reproducibility of the assays (Carneiro et al., 2019; Holzinger et al., 2014; Huizhi et al., 2008; Iglesias-Mayor et al., 2019; Toyos-Rodríguez et al., 2020). Their use as labels in immunosensing has been deeply studied, constituting an outstanding alternative to traditionally used enzymes (de la Escosura-Muñiz et al., 2008, 2010a; de la Escosura-Muñiz and Merkoçi, 2010; Lara and Pérez-Potti, 2018).

In this context, metal nanoparticles have emerged due to their catalytic potential, making them reporters with an outsized sensitivity that is associated with their high surface-to-volume ratios, high mechanical strength and ease of functionalization (Doria et al., 2012; Wittenberg and Haynes, 2009). From all metal nanoparticles, gold nanoparticles are chiefly used. However, in most cases their detection requires the use of highly acidic media, as it is the case of their use as catalysts of hydrogen evolution reaction (HER) (Baptista-Pires et al., 2019; de la Escosura-Muñiz et al., 2015, 2010b; Hassan et al., 2015; Maltez-da Costa et al., 2012, 2010). However, this extra requisite results the incorporation of additional steps that increase the time of analysis. For this, the use of alternative nanoparticles capable of acting as catalysts at neutral pH has been recently explored (Cao et al., 2020; Iglesias-Mayor et al., 2020; Rivas et al., 2014).

The use of alternative nanoparticles is based on the catalysis of reactions that naturally take place at neutral pH, as water oxidation reaction (WOR) or oxygen reduction reaction (ORR). ORR is one of the most studied electrocatalytic reactions as it plays a pivotal role in the electrochemical energy conversion (Maduraiveeran, 2021; Rahman et al., 2021; Rößner and Armbrüster, 2019; Tian et al., 2020). This cathodic electrode reaction is a complicated and slow process in which various reaction intermediates are embedded. Thus, the reduction of O_2 has been proposed to take place following two different pathways: a straightforward four electron reaction (1) or an indirect process called the two electron process (2) (Han et al., 2009; Lim and Wilcox, 2012; Tammeveski et al., 2012; Wang et al., 2021).

$$O_2 + 2H_2O + 4e^- = 4OH^- \quad (1)$$

$$O_2 + H_2O + 2e^- = HO_2^- + OH^- \quad (2)$$

The role of metals such as palladium, platinum or silver has been related to the formation first of a superoxide ion ($O_2 + e^- = O_2^{\bullet -}$) (Kusunoki et al., 2021; Singh and Buttry, 2012; Spendelow and Wieckowski, 2007).

Platinum (Pt) catalysts have been the benchmark in the ORR catalysis owing to their durability in acidic media and their high activity (Nørskov et al., 2004). However, their high cost is their main drawback. Therefore, the use of other metals has been postulated as an alternatively cheaper catalyst that also boosts ORR activation (Tian et al., 2020).

In this context, palladium (Pd) as a metal has been proven to be as promising as Pt alloy (Wang et al., 2015a, 2015b; Wu et al., 2021) or in combination with other metals. Zhang et al. (2012), described the combination of Pd and Au in a crown-jewel structure with a hexagonal Pd core decorated with upper Au atoms mimicking the disposition of a crown. The selective introduction of upper Au atoms in the vertex and corners of the Pd core, provided a synergistic effect increasing the intrinsic catalytic activity of Pd, as shown toward the glucose oxidation and H_2O_2 decomposition reactions.

In this context, the objective of this work is to explore for the first time the role that the introduction of increasing concentrations of Au into Pd nanoclusters have in their electrocatalytic activity toward the oxygen reduction reaction (ORR). A careful control of the amount of Au atoms introduced in the cluster and the evaluation of the optimum Pd: Au ratio for getting the maximum catalytic activity is a key study, missing in the bibliography. This may be of great interest not only for biosensing, but also for applications such as energy converting on fuel cells.

As a proof-of-concept of application in biosensing, the synthesized Pd-AuNPs prepared with an optimum Pd/Au rate have been used as tags in a magnetic bead-based immunoassay for the detection of hyaluronidase, a chronic wound infection biomarker. Chronic wounds represent an important healthcare challenge that affects 1–2% of population in developed countries, a number that it is expected to increase in association to the rise in life expectancy and the establishment of a more sedentary lifestyle (Clinton and Carter, 2015; Järbrink et al., 2016). Chronic wounds lack from healing and infection is a common complication that worsens the situation, prolonging pain and morbidity in patients and requiring long hospitalization periods (Han and Ceilley, 2017; Verbanic et al., 2020). Nosocomial pathogens as Gram-positive *Staphylococcus aureus* or *Enterococcus faecium and* Gram-negative *Pseudomonas aeruginosa* proliferate in chronic wounds, so that their identification to certain stain is required for antibiotic administration (Han et al., 2011; Schmidtchen, Helene Wolff, Carita H, 2001; Serra et al., 2015; Zhou et al., 2020). However, actual identification of infection is based on culture techniques and gold-standard biopsy, both invasive and time-consuming procedures, so as the development of alternative tools for a rapid diagnosis is desirable (de la Escosura-Muñiz et al., 2019; Han et al., 2011; Mahnic et al., 2021; Melendez et al., 2010). In this context, several biomarkers such us hyaluronidase have been identified as virulence factors. Hyaluronidase is produced by the main pathogenic Gram-positive bacteria that colonize mucosal surfaces and skin, although its role is still being investigated (Hynes and Walton, 2000). Even though there are human hyaluronidases, bacterial ones (EC 4.2.2.1 or EC 4.2.99.1) are characterized by producing unsaturated disaccharides through endo-N-acetylhexosaminidase activity (Stern and Jedrzejas, 2006). This bacterial specificity makes hyaluronidase a potential biomarker of infection in chronic wounds, also allowing to discern between bacterial genders.

In addition to the unprecedented study related to the effect of the Pd: Au ratio on the electrocatalytic activity toward the ORR, to the best of our knowledge, this is the first time that this type of bimetallic NPs are used as tags in biosensing, taking advantage of such property.

2. Experimental

2.1. Reagents and equipment

Palladium (II) chloride ≥ 99.9%, polyvinylpyrrolidone mol wt 40.000, gold (III) chloride trihydrate 99.9%, gold nanoparticles (5 nm diameter), albumin from bovine serum (BSA), human IgG and lysozyme from chicken egg white were purchased from Sigma-Aldrich (Spain). Ethanol dried (max 0.01% H_2O), tri-sodium citrate trihydrate and Tween-20 detergent were supplied by Merk Millipore (Spain).

Hyaluronidase recombinant protein, monoclonal biotin-linked antibody to hyaluronidase (epitope aa60-159) and polyclonal antibody to hyaluronidase (epitope N-terminal region) were supplied by MyBioSource (USA). As described, both antibodies are able to recognize different epitopes of the hyaluronidase protein.

Streptavidin-modified magnetic beads (M-280) were obtained from Thermo Fisher Scientific (Spain).

Ultrapure water (18.2 MΩ cm @ 25 °C) taken from a Millipore Direct-Q 3 UV purification system purchased from Millipore Ibérica S.A. (Spain) was used for the preparation of the solutions, unless otherwise stated.

Phosphate buffer electrolyte solutions used for the immunoassay

were composed of sodium chloride, potassium chloride, disodium hydrogen phosphate and potassium dihydrogen phosphate all provided by Merck (Germany).

For the immunoassay, two main buffers were used: binding and washing (B&W) buffer (0.1 M PBS pH 7.2 with 0.05% (v/v) Tween-20) and blocking buffer (BB) (0.1 M PBS pH 7.2 with 5% (w/v) BSA).

2.2. Instrumentation

High-resolution transmission electron microscopy (HRTEM) analysis was performed using a JEOL-JEM 2100f operated at 200 kV with a resolution of 1.9 Å between points and 1.0 Å between lines to determine the particle size distribution of the synthesized NPs. Elemental analysis of the corresponding NPs was performed relying on an energy-dispersive X-ray microanalyzer EDX (X-max, Oxford Instruments, Abingdon, UK) coupled to a bright-field detector (EM24541SIOD, JEOL) for use in the STEM mode, together with the use of INCA software (ETAS S.A.S., Saint-Ouen, France).

For the immunoassay, a MagRack® 6 from Sigma-Aldrich (Spain), a MSC-100 cooling thermo shaker from Labolan (Spain) and a thermostatic centrifuge (Rotanta 460 R) from Hettich (Germany) were used.

For the electrochemical characterization, a μAutolab type II with Autolab GPES software from Metrohm (Switzerland) was used. As electrodes, screen-printed carbon electrodes (SPCEs, ref DRP-110) with a working and counter carbon electrode and a silver pseudoreference electrode were used and they were connected to the potentiostat by a specific connector (ref. DRP-DSC) provided by Metrohm DropSens S.L. (Spain). For measuring the immunosandwich assay, a magnetic support for SPEs (DRP-MAGNET-700) (Metrohm DropSens S.L. (Spain)) was used.

2.3. Synthesis, bioconjugation and characterization of Pd-AuNPs

The synthesis of Pd nanoclusters was performed following a previously reported procedure with some modifications (Zhang et al., 2012). Briefly, 50 mL of a suspension of 0.66 mM palladium (II) chloride prepared in ethanol: water (1:3) were vigorously stirred in a round bottom flask at room temperature for 15 min. Then, 50 mL of a PVP 66 mM solution in ethanol: water (1:3) were added, and the suspension was again stirred at room temperature for additional 15 min. Afterwards, the suspension was heated at 100 °C for 2h under reflux and inert atmosphere (Ar, Ar ≥ 99,999, ALPHAGAZ™ 1, from AirLiquid, Spain). The final product was purified with centrifugation at 4000*g*, 20 °C for 30 min using Amicons® with a cut-off value of 10.000 molecular weight. Three washing steps with water and one with ethanol, using the same Amicons® were also done. Then, the remaining ethanol was evaporated, and the final product was resuspended in a 1:3 ethanol: water solution to a final concentration of 0.66 mM Pd.

For the selective introduction of gold, 20 mL of a gold (III) chloride trihydrate solution (0.135 mM, 0.735 mM, 0.835 mM, 0.935 mM or 1.135 mM) were poured into a round bottom flask containing the obtained Pd nanoclusters. The solution was heated for 30 min at 100 °C under reflux and inert atmosphere. In order to reduce aggregation, 2 mL of tri-sodium citrate in a concentration of 0.17 M were introduced in the flask and the solution was purified by centrifugation at 8000*g*, 4 °C for 45 min using LoBind tubes. Then, the remaining pellet was washed three times with water by centrifuging at 8000 g, 20 °C during 30 min.

The final product was resuspended to a final concentration of 1.45×10^{12} NPs/mL according to Nanoparticle tracking analysis (NTA) measurements.

Meanwhile, 690 μL of the Pd-AuNPs suspension were transferred into a 1.5 mL LoBind Eppendorf® tube and centrifuged at 7500 g, 20 °C for 20 min with the addition of 10 μL of 1.75% Tween-20. After centrifugation, the pellet was resuspended in 700 μL of 2 mM trisodium citrate pH 7.4 solution. Then, 57.5 μL of 50 μg/mL solution of a polyclonal antibody anti-hyaluronidase were added and incubated for 1 h at 650 rpm, 25 °C. For purification, the solution was centrifuged at 7500 g, 4 °C for 15 min, the supernatant was removed, and the pellet resuspended in 0.1M PBS pH 7.2 with 1% BSA.

2.4. Electrochemical measurements

The electrocatalytic activity of the obtained Pd and Pd-AuNPs toward the ORR was electrochemically evaluated by dropping 10 μL of the NP suspension onto the working electrode of an SPCE. Then, the solution was kept until complete absorption, when 40 μL of 10 mM PBS pH 7.4 were added. For obtaining the background signals, 50 μL of a 10 mM PBS pH 7.4 solution were used. Linear sweep voltammogram (LSV) scans were recorded in the range from 0 V to −0.8 V at a scan rate of 0.1 V/s.

Chronoamperometric scans were obtained maintaining a fixed potential of −0.45V for 50s. Signal at 5s was selected as analytical signal for the evaluation of the electrocatalytic activity of the different Pd-AuNPs toward the ORR and for the quantitative studies.

In all the experiments, measurements were performed by triplicate at room temperature, using a different SPCE.

2.5. Immunoassay for the detection of hyaluronidase wound infection biomarker

Hyaluronidase was detected using magnetic bead (MB) platforms and Pd-AuNPs tags, adapting a previously reported immunoassay format (Iglesias-Mayor et al., 2020). Briefly, 15 μL (10 mg/mL) of commercially available streptavidin-modified MBs were conveyed to a 0.5 mL LoBind Eppendorf tube, and washed three times with B&W buffer. Then, MBs were resuspended in 135 μL of B&W buffer and 15 μL of 15 μg/mL biotin-linked monoclonal anti-hyaluronidase antibody were added, and the solution was incubated for 30 min at 25 °C, 650 rpm in a thermo shaker incubator. Past this time, the excess of biotin-linked monoclonal anti-hyaluronidase antibody was removed with the help of a MagRack®, and the solution was washed three-times with B&W buffer. Then, 150 μL of blocking buffer (PBS 0.1 M pH 7.2 with 5% BSA) were added to each tube and incubated for 1 h at the same heating and stirring conditions to minimize unspecific absorptions.

Once the MBs-anti hyaluronidase conjugate was obtained, 100 μL of hyaluronidase solutions ranging from 0 to 4600 ng/mL were added and incubated for 30 min at 25 °C, 650 rpm. The final product was washed three times with B&W buffer.

Then, 150 μL of the Pd-AuNP conjugate were added to with the MBs final conjugate and incubated for 1h at 25 °C and 650 rpm. The resulting immunocomplex was washed twice with B&W buffer and twice with 10 mM PBS pH 7.4 and reconstituted in 150 μL of this buffer. The final conjugate was chronoamperometrically measured by placing 40 μL of the final solution on the working area of a SPCEs (with a magnetic support on the reverse side) and applying a voltage of −0.45 V for 50 s, being the value of the current recorded at 5 s selected as analytical signal.

Selectivity was evaluated following the above detailed procedure but with the addition of solutions at 750 ng/mL of albumin from bovine serum (BSA), immunoglobulin G (IgG) or lysozyme (Lys) instead of 750 ng/mL hyaluronidase. Exudates from patients with both sterile and infected ulcers were also measured following the same immunoassay procedure than the detailed for the hyaluronidase standard solutions. Both control and infected swabs were provided by the Chronic Ulcers Unit of the Hospital Universitario Central de Asturias (HUCA), where they were analyzed by traditional culture techniques in order to corroborate the presence of bacterial infection in the infected swab.

3. Results and discussion

3.1. Characterization of the PdNPs and Pd-AuNPs with different Pd/Au content

Pd-AuNPs were prepared adapting a previously described procedure consisting in the selective introduction of Au atoms on vertex or corner positions of Pd nanocluster, following a galvanic replacement reaction (Fig. 1). The obtained PdNPs follow a "crown-jewel" model that was first described by Zhang et al. (2012), being this name related to the decoration that Au atoms do in the PdNPs, acting as jewels decorating a crown. This method is based on the synthesis of PdNPs, prepared by alcohol reduction in the presence of polyvinylpyrrolidone, and the subsequent introduction of Au atoms on top positions rather than sheltering the PdNPs. The introduction of Au atoms in these positions has been previously attributed to the difference in free energies associated to top, edges and face atoms of a cluster, that affect the preference of Au atoms to occupy first top positions (Campbell, 2004; Toshima et al., 2005; Zhang et al., 2012).

The presence of both metals has a synergistic effect that increases their electrocatalytic activity. Moreover, the presence of external Au atoms facilitates the further conjugation of the obtained Pd-AuNPs with antibodies, owing to the Au affinity to the cysteine groups that are present in the immunoglobulin structure (Ambrosi et al., 2007; Brust et al., 1994).

Pd-AuNPs prepared with 0.835 mM $HAuCl_4$ were selected as representative for their comparison with the starting PdNPs. High resolution-transmission electron microscopy (HRTEM) (Fig. 2A and B) characterization showed spherical nanoparticles with a diameter of 4 ± 1 nm for the PdNPs, while a slight increase in the size to 5 ± 1 nm was noticed for Pd-AuNPs. It is worthy to mention that a slight aggregation is observed compared to initial PdNPs, probably due to the introduction of Au. Nevertheless, we observed that the introduction of tri-sodium citrate after the synthesis seems to regulate this effect. Moreover, STEM-TEM mode EDX analysis demonstrated the presence of both Pd and Au in the Pd-AuNPs structure, as expected (Fig. 2C-D-E).

The selective introduction of increasing amounts of Au slightly leads to the galvanic replacement of Pd surface atoms by Au atoms, leading to a higher covering and affecting the electrocatalytic activity of the final NPs. So bimetallic Pd-AuNPs were prepared by adding $HAuCl_4$ solutions at different concentrations ranging from 0.135 mM to 1.135 mM to the Pd nanocluster. The average elemental analysis done relying on EDX spectroscopy of the obtained Pd-AuNPs confirmed the presence of increasing proportions of Au on the NPs with increasing the incorporated Au concentration in the reaction (Table 1). This continued to be the case until reaching equal proportions of Pd and Au.

3.2. Evaluation of the electrocatalytic activity of Pd-AuNPs toward the oxygen reduction reaction (ORR): effect of the selective introduction of Au atoms in the Pd nanocluster

The electrocatalytic activity of the synthesized Pd-AuNPs toward the oxygen reduction reaction (ORR) was first evaluated by lineal sweep voltammetry (LSV) on SPCEs. LSV scans were recorded from 0 to −0.8V in PBS 10 mM pH 7.4 at a scan rate of 0.1 V/s. Pd-AuNP-3 (as described in Table 1) were chosen for this study, being the results compared with those obtained for the unmodified PdNPs. Commercial AuNPs of 5 nm in diameter were also evaluated for comparison purposes (Fig. 3). NPs concentration was 1.45×10^{12} NPs/mL in all cases.

The background (curve a) reveals that the oxygen reduction starts at approximately −0.70 V, and this value slightly shifts to −0.55 V in the presence of AuNPs (curve b). A notable shift of the half-wave potential to around −0.47 V is noticed for PdNPs, also noticing an increase in the associated current. Interestingly, this effect is dramatically enhanced for the Pd-AuNP-3, where the potential shifts to around −0.18 V, accompanied with a high increase in the associated current. This behaviour is in agreement with what was expected, due to the synergy in the catalytic activity of bimetallic NPs (Sha et al., 2019; Tang and Tang, 2015; Wang et al., 2013; Zhao and Xu, 2006), which assist on the cleavage of the O═O bond, lowering the energy barrier (Ma et al., 2019) of such intermediate.

Once corroborated the higher electrocatalytic activity of the bimetallic Pd-AuNPs compared with the individual PdNPs and AuNPs, the effect of the selective introduction of Au atoms in the Pd nanocluster was studied, taking advantage of the chronoamperometric mode due to its high sensitivity, simplicity and speed. In agreement, with what was observed in the LSV study, a fix potential of −0.45 V was selected for the chronoamperometric measurements, being it applied for 50 s (Fig. 4A). The absolute value of the current generated at 5 s (response time of the sensor; current profiles were not stable for shorter times) was chosen as the analytical signal used for the comparison between the different Pd-AuNPs prepared (Fig. 4B). As observed, the NPs with only a 12% of Au (Pd-AuNP-1), give an absolute electrocatalytic current similar to that of the PdNPs cluster (around 11 μA). This suggests that although Au atoms are first introduced in the more reactive top positions (vertex and corner) of the cluster, due to the lower free energies of such atoms, this small amount is not enough to significantly enhance the catalytic activity of the Pd nanocluster. However, a dramatic increase in the absolute signal (to approx. 34 μA) is observed for the NPs with a 21% of Au (Pd-AuNP-2). A slight increase in the signal (to approx. 38 μA) is then observed when increasing the Au content to 30% (Pd-AuNP-3). Interestingly, increasing amounts of Au in the nanocluster (44% for Pd-AuNP-4 and 54% for Pd-AuNP-5) exert the opposite effect. These results indicate that the maximum synergy between both metals is reached for a Pd:Au ratio of approximately 2.3:1. The majority presence of the Au atoms in the vertex and corner positions of the cluster, with a high degree of coordinative unsaturation, makes them available for participating in the ORR reaction, also being responsible of such effect. in such positions of the cluster. However, for increasing amounts of Au synergy begins to lose, dominating the presence of Au, which is a worse catalyst than Pd, as corroborated by the small current (1.54 μA) recorded for AuNPs.

According to these results, Pd-AuNP-3 were selected for their further use as electrocatalytic labels in biosensing. Before that, the ability of our

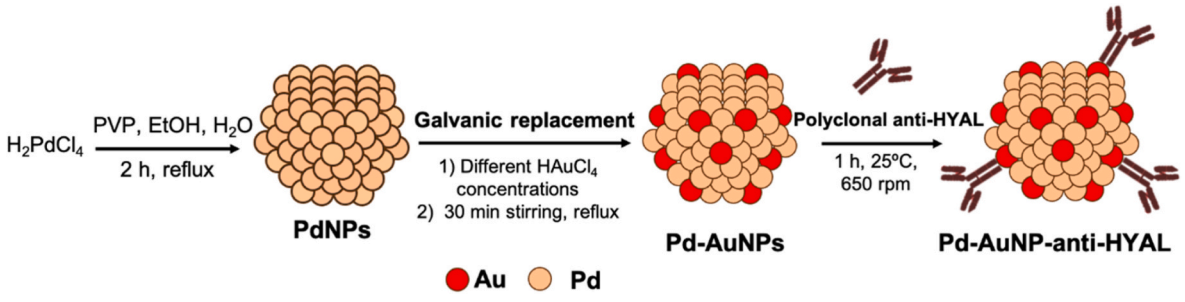

Fig. 1. Schematic representation of PdNPs and Pd-AuNPs synthesis and further conjugation with polyclonal anti-hyaluronidase (HYAL) antibodies.

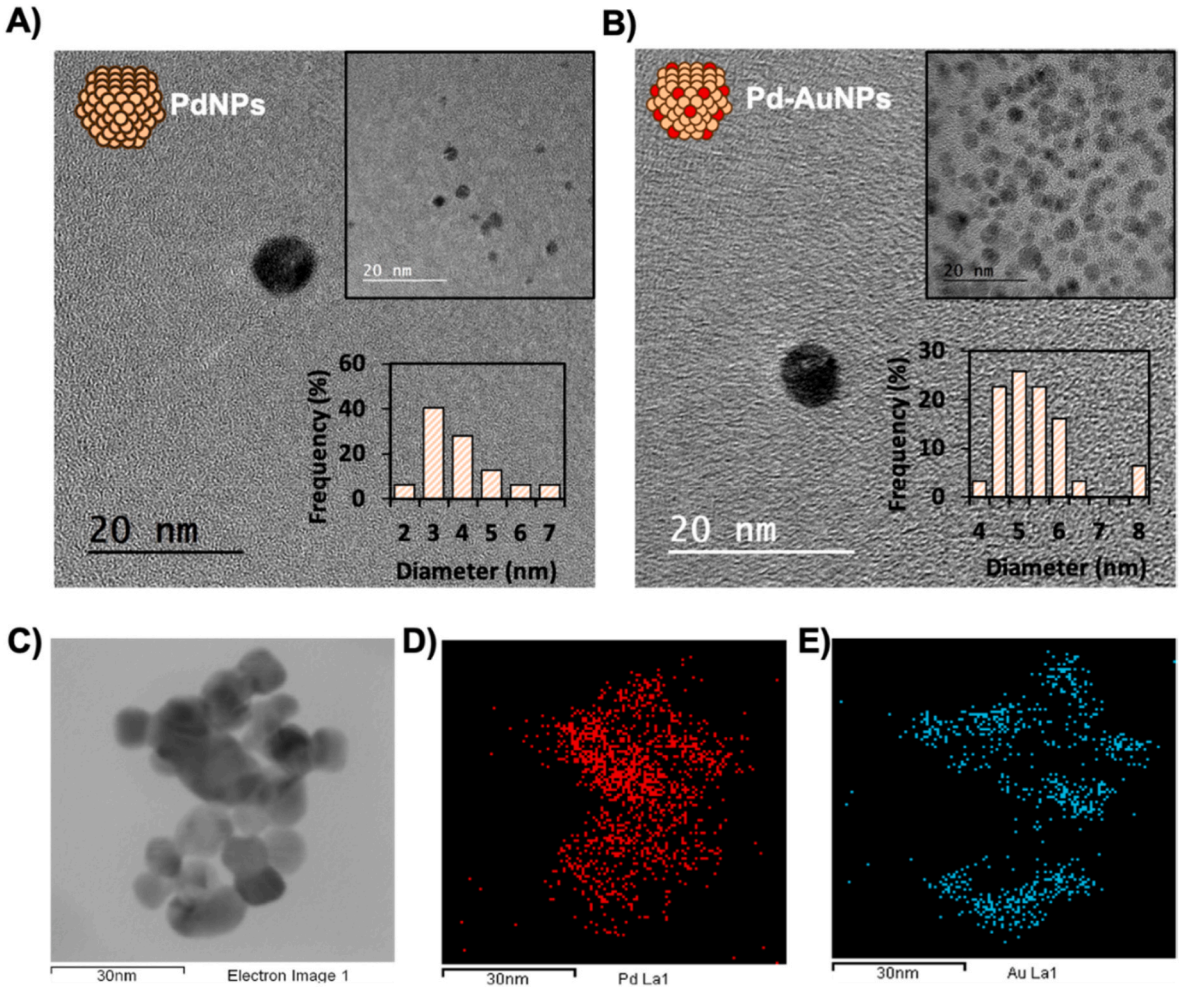

Fig. 2. HRTEM micrographs for PdNPs (**A**) and Pd-AuNP (**B**) (prepared with 0.835 mM $HAuCl_4$) and their particle size distribution analysis (insets); The difference in the particle density observed in both pictures is due to the different samples dilution used for the analysis. **C**. Bright-field STEM micrograph showing Pd-AuNPs with the performed EDX area maps showing the presence of Pd elements (**D**) and Au elements (**E**).

Table 1
Summary of the different synthesized Pd-AuNPs and characterization in terms of their Pd and Au average composition obtained through STEM-EDX analysis. Data are given as average ± SD (n = 5).

		STEM-EDX analysis	
Sample	[$HAuCl_4$] (mM)	% Pd atom	% Au atom
Pd-AuNP-1	0.135	97 ± 1	3 ± 1
Pd-AuNP-2	0.735	83 ± 6	17 ± 3
Pd-AuNP-3	0.835	70 ± 3	30 ± 3
Pd-AuNP-4	0.935	56 ± 16	44 ± 16
Pd-AuNP-5	1.135	48 ± 3	52 ± 3

electroanalytical method to quantify small amounts of such NPs was evaluated. Chronoamperometry, under the same conditions than the described above, was also selected for such quantitative studies. As observed in Fig. 5A, a proportional increase of catalytic cathodic current was observed with corresponding increases in the concentration of Pd-AuNP-3. As shown in Fig. 5B, a linear relationship between the analytical signal (current recorded at 5 s) and the Pd-AuNP-3 concentration was found in the range between 1×10^{10} and 1.2×10^{11} NPs/mL, adjusted to the following equation:

$$|Current_{5s}| \, (\mu A) = 1.63 \times 10^{-10} \, [\text{Pd-AuNP-3}] \, (\text{NPs/mL}) - 0.05$$

The calibration curve presented a good correlation coefficient (r) of 0.9985 and reproducibility, with a standard deviation below 8.0% (n = 3). The limit of detection (LOD), calculated as three times the standard deviation of the intercepted divided by the slope, was of 5.97×10^9 NPs/mL.

3.3. Electrocatalytic detection of hyaluronidase wound infection biomarker using Pd-AuNP tags

Hyaluronidase is an enzyme secreted as virulence factor by Gram-positive bacteria during a chronic wound infection. Hyaluronidase detection is useful for the identification of bacterial infection to provide the patients with the correct antibiotic treatment and thus reducing any bacterial antibiotic resistances. As a proof-of-concept of the suitability of the high electrocatalytically active Pd-AuNP-3 as labels, an immunosensor for the detection of hyaluronidase was developed. In this context, the evaluation of the Pd-AuNP-3 activity after conjugation with antibodies is of key relevance for the further biosensing application. As observed in Fig. 6A, such Pd-AuNP-3/antibody conjugate retained most of the catalytic activity, allowing for its use as an electrochemical tag. The little decrease in activity compared with bare Pd-AuNP-3 could be attributed to a partial blocking of the Au surface by the antibodies, which might somehow affect the synergy between both metals. This behavior was previously observed for other metallic and bimetallic NPs catalyzing different reactions (i.e. de la Escosura-Muñiz et al., 2009; Iglesias-Mayor et al., 2020).

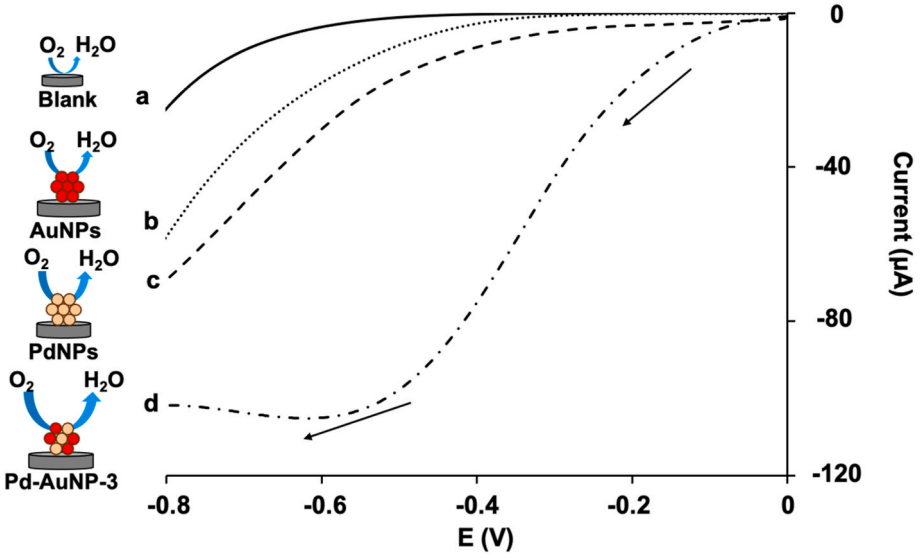

Fig. 3. Lineal sweep voltammograms (LSV) recorded from 0 to −0.8 V at a scan rate of 0.1 V/s in 10 mM PBS pH 7.4, for a bare electrode (background; a) and for electrodes modified with AuNPs (b), PdNPs (c) and Pd-AuNP-3 (d). NPs concentration: 1.45×10^{12} NPs/mL.

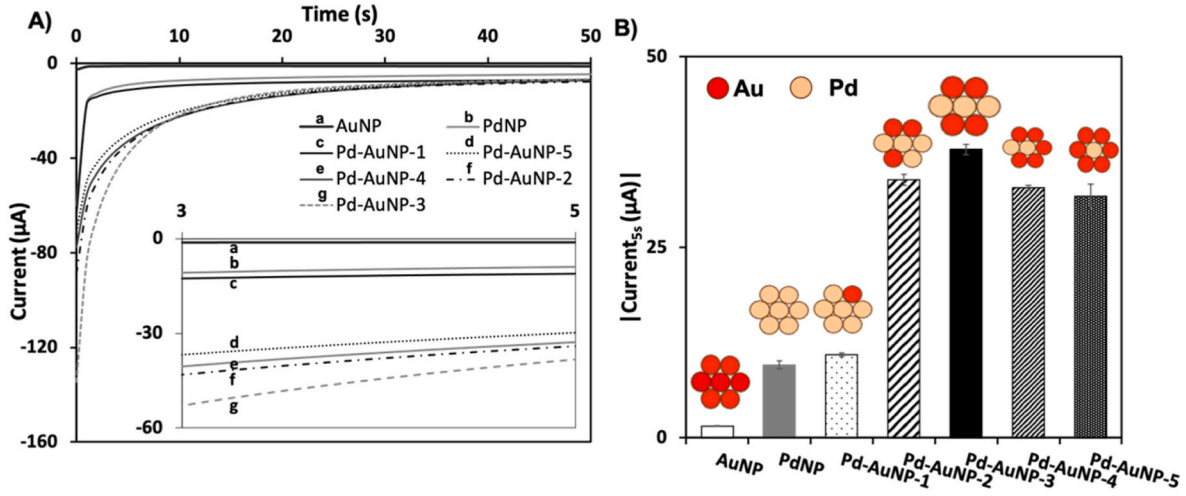

Fig. 4. Electrochemical characterization of Pd-AuNPs with different Au content. **A.** Chronoamperograms recorded at −0.45 V for 50 s in PBS 10 mM pH 7.4 for AuNPs (a), PdNPs (b), Pd-AuNP-1 (c), Pd-AuNP-2 (f), Pd-AuNP-3 (g), Pd-AuNP-4 (e) and Pd-AuNP-5 (d). Inset corresponds to the region from 3s to 5s and from 0 μA to −60 μA. **B.** Comparison of the analytical signal (absolute value of current recorded at 5 s) for each NPs. Data are given as average ± SD (n = 3). NPs concentration: 1.45×10^{12} NPs/mL. NPs composition as detailed in Table 1.

The developed immunosensor takes advantage of the use of MB as platforms to facilitate separation and minimizing matrix effects (Ahmadi et al., 2021; de la Escosura-Muñiz et al., 2016) (Fig. 6B). The advantages of the MB-based immunoassays are well-known. First, the fact that the reactions take place in liquid phase, with stirring, allows to improve their kinetics, reducing the incubation times to approximately 20 min (typically 90 min for assays performed in solid phase). The magnetic separation performed after each incubation step also allows to pre-concentrate the sample, which leads to improved sensitivities. Moreover, such separation after capturing the analyte allows to remove the rest of compounds present in the sample which may interfere in the electrochemical measurement. This leads to a reduction of matrix effects and to an increase in selectivity.

Briefly, biotinylated monoclonal anti-hyaluronidase antibody (biotin anti-HYAL) was immobilized onto streptavidin-modified commercial magnetic beads and the conjugate was incubated with increasing concentrations of hyaluronidase. The resulting complex was put in contact with the MBs-hyaluronidase conjugate, forming the final immunosandwich. The use of antibodies as recognition elements confers the immunosensor with selectivity against hyaluronidase.

The resulting complex was placed on a SPCE, to which working electrode was attracted by the action of a small external magnet placed on its reverse side. The analytical method consists in applying a potential of −0.45 V in chronoamperometric mode and measuring the current recorded at 5 s (analytical signal), as optimized for the Pd-AuNP-3 determination.

The absolute value of this current increases with the Pd-AuNP-3 concentration, due to their catalytic activity toward the ORR. So, when higher is the concentration of hyaluronidase in the immunoassay, higher is the amount of the Pd-AuNPs-3 tags, being the signals correlated with the analyte concentration, as shown in Fig. 7A.

Dose-response experiments were performed in the range of 125–4600 ng/mL of hyaluronidase with a good linear relationship (r = 0.9982) according to the following equation:

$$|\text{Current}_{5s}| \text{ (μA)} = 0.003 \text{ [Hyaluronidase] (ng/mL)} + 0.4432$$

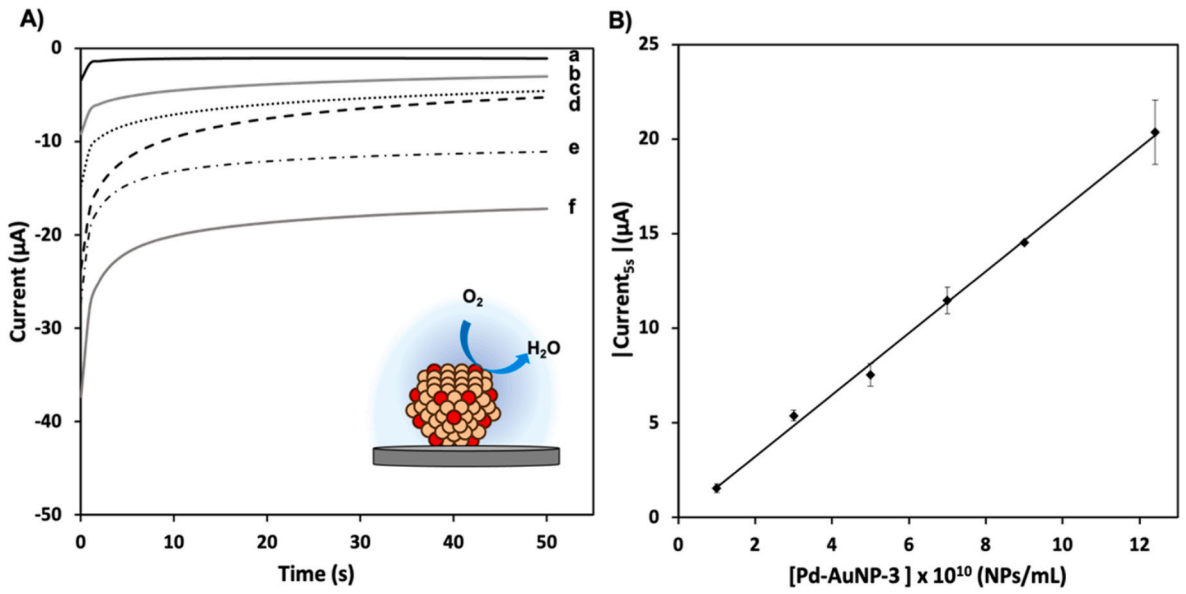

Fig. 5. A. Chronoamperograms recorded at −0.45 V during 50 s in 10 mM PBS pH 7.4 for increasing concentrations of Pd-AuNP-3: 1.00 × 10^{10} NPs/mL (a), 3.00 × 10^{10} NPs/mL (b), 5.00 × 10^{10} NPs/mL (c), 7.00 × 10^{10} NPs/mL (d), 9.00 × 10^{10} NPs/mL (e) and 1.20 × 10^{11} NPs/mL (f). **B.** Relationship between the analytical signal (current at 5 s) and Pd-AuNP-3 concentration. Data are given as average ± SD (n = 3).

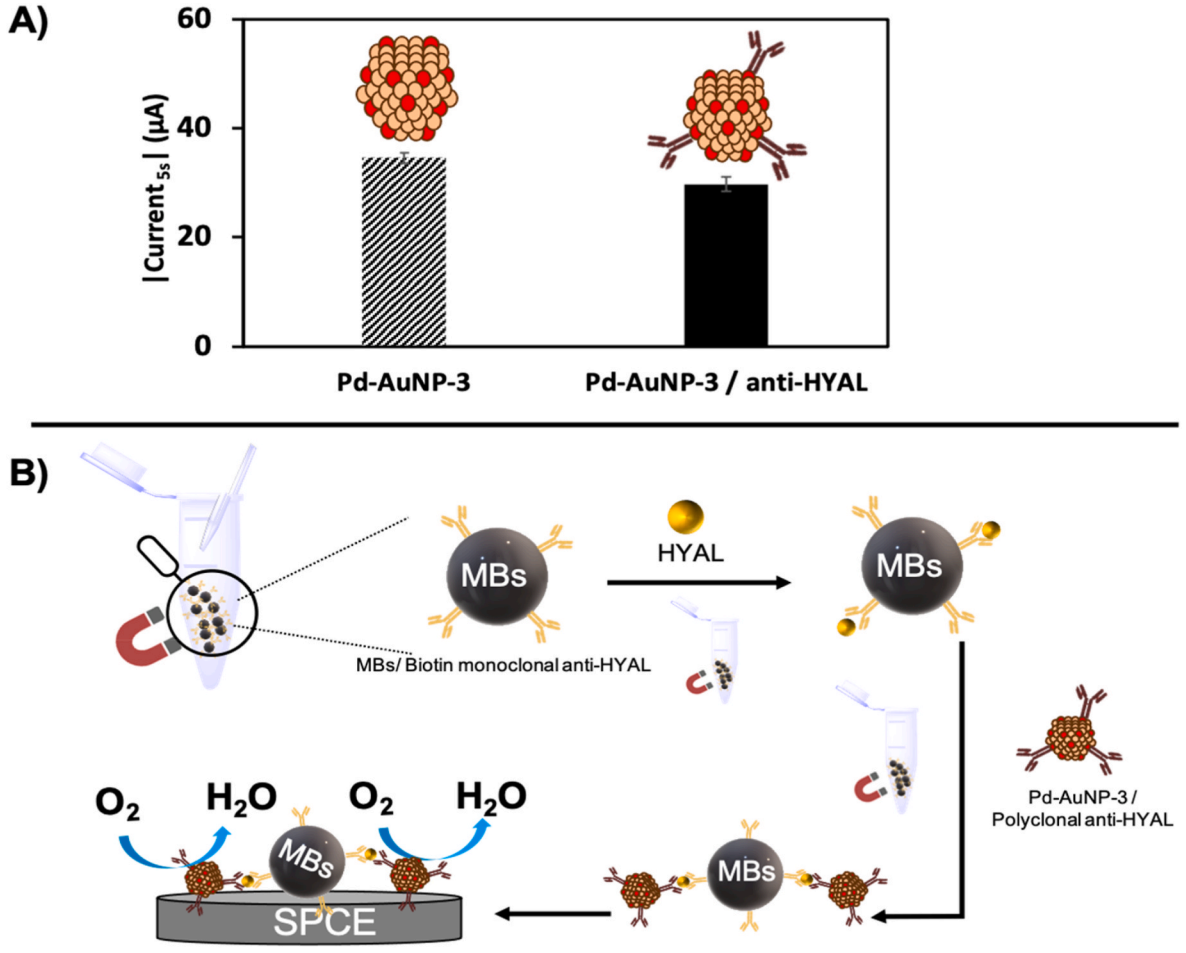

Fig. 6. A. Comparison of the analytical signals (coming from chronoamperograms obtained applying a potential of −0.45 V and measuring the current recorded at 5 s) for Pd-AuNP-3 and Pd-AuNP-3/anti-HYAL conjugate. Data are given as average ± SD (n = 3). **B.** Schematic representation of the immunosensor developed for the detection of hyaluronidase (HYAL) using Pd-AuNP-3 tags and magnetic beads (MBs) platforms.

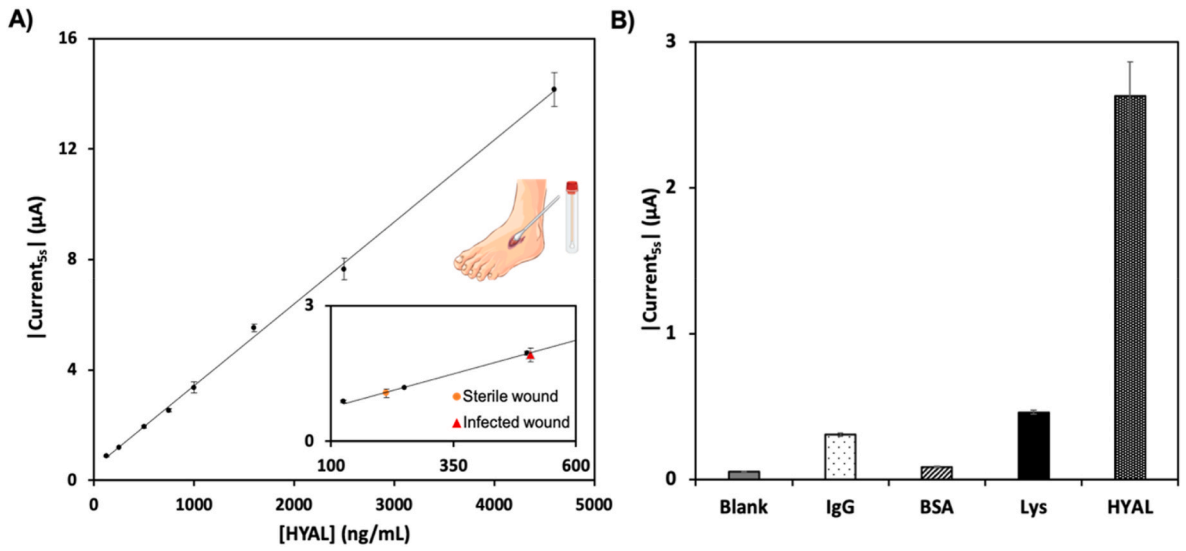

Fig. 7. A. Calibration plot signals (coming from chronoamperograms obtained applying a potential of −0.45 V and measuring the current recorded at 5 s) obtained for standard solutions of hyaluronidase (from 125 to 4600 ng/mL) as well as the analytical signals obtained for swab exudates from patients with sterile (circle) and infected (triangle) ulcers (inset). Data are given as average ± SD (n = 3). **B.** Sensor response to different potential interferences, all of them at a concentration of 750 ng/mL. Data are given as average ± SD (n = 3).

The obtained LOD, calculated as three-times the SD of the intercepted divided by the slope was 50 ng/mL, equivalent to 0.02 U/mL (437 U/mg). The reproducibility of the method was also good with an RSD below 8% (n = 3).

The obtained LOD is one of the lowest found in the biosensors-related bibliography (Table 2), demonstrating the excellent performance of our method based on the use of Pd-AuNP-3 tags.

3.4. Selectivity studies and hyaluronidase determination in chronic wound exudates

Bacterial identification in chronic wound exudates in a short time and with a high selectivity is desirable for achieving a better screening methodology in wound infection handling. For that reason, attaining an analytical method with a high selectivity and good performance in real samples is advantageous. In this context, the use of MBs in the here developed immunosensor supposes a major advantage as they allow to separate biomolecules from complex samples, reducing matrix effects (Ahmadi et al., 2021; de la Escosura-Muñiz et al., 2016).

Selectivity of the Pd-AuNP-3 based immunosensor was evaluated against common analytes present in human samples, as it is BSA, IgG and lysozyme, another well-known infection biomarker (Hasmann et al., 2011; Mota et al., 2021; Silva et al., 2020). Analytical signals recorded for each condition were insignificant comparing with hyaluronidase (Fig. 7B), even in the presence of common wound exudate biomolecules as lysozyme. Thus, the Pd-AuNP-3/MBs based immunosensor had enhanced selectivity to hyaluronidase sensing without significant interferences.

Moreover, the immunosensor was evaluated in real samples obtained from exudates of patients with open wounds, being one from a patient with a sterile wound and the other one from an infected wound (Fig. 7A, inset). The hyaluronidase concentration was directly extrapolated from the calibration curve, considering the low matrix effects observed in the presence of MBs. It can be clearly observed a difference between the hyaluronidase concentration detected in a clean (213 ± 18 ng/mL; 0.09 ± 0.008 U/mL) and an infected wound (507 ± 40 ng/mL; 0.22 ± 0.017 U/mL), attesting the suitability of the immunosensor to discriminate between them.

These levels are much lower than the provided by the gold standard turbidimetric assay, which has a linear range from 2 to 5 U/mL (Chen et al., 2020). This makes it difficult to apply this method for validation. In addition, turbidimetric method requires a complex methodology that implies the use of hyaluronic acid for the enzymatic reaction, in contrast with the simplicity of our immunosensor.

Moreover, there is not a clear consensus in bibliography about the expected levels of hyaluronidase in infected and non-infected samples.

Table 2
Comparison with other reported biosensors for hyaluronidase detection.

Sensing principle	Transduction technique	Limit of detection (U/mL)	Sample	Ref
Bimetallic gold/silver nanoclusters-gold nanoparticles as fluorescence quencher	Fluorescence	0.3	Spike and recovery	Liu et al. (2019)
Conjugated polymer nanoparticles and Au nanorods	Fluorescence	0.003	Spike and recovery	Wang et al. (2022)
Water soluble fluorescence molybdenum disulfide quantum dots quenched by hyaluronic acid gold nanoparticles	Fluorescence	0.7	Spike and recovery	Gu et al. (2016)
Carbon Dot/Naphthalimide and hyaluronic acid Förster resonance energy transfer (FRET) mechanism	Fluorescence	0.09	Not tested	Raj et al. (2021)
Electrostatic interaction between hyaluronic acid and $Ru(bpy)_3^{2+}$	Electrochemiluminiscence	0.33	Spike and recovery	Li et al. (2018)
Methylene blue-hyaluronic acid complexes and enzymolysis through hyaluronidase	Differential pulse voltammetry (DPV)	0.28	Urine samples	Li et al. (2021)
Nanopores blocking by hyaluronidase	Differential pulse voltammetry (DPV)	64	Bacteria culture	de la Escosura-Muñiz et al. (2019)
Pd-AuNP-3 /MB immunosensor based on electrocatalytic activity toward the ORR	Chronoamperometry	0.02	Exudates from human wounds	This work

Considering this, and the limitations of the turbidimetric assay, our immunosensor provides a useful tool for further carefully evaluation in a high number of patient samples. A threshold value for discriminating infected and non-infected samples should be further defined for a practical application of this method in a real scenario.

4. Conclusions

In this work, we study for the first time the role that slight changes into the Pd/Au proportion have in the electrocatalytic activity of bimetallic Pd-AuNPs toward the oxygen reduction reaction (ORR), together with their application as novel tags for the determination of an infection biomarker in chronic wound exudates.

The selective introduction of gold atoms on the palladium nanocluster, following a galvanic substitution procedure, is quantitatively evaluated by STEM-EDX analysis. Our findings indicate that, the synergy between both metals is strongly enhanced when the amount of gold is controlled and occupies the more reactive positions of the cluster, affecting the obtained electrocatalytic activity. This is of key relevance, since it is observed that an excess of gold leads to a decrease in such activity. These findings may be of great interest not only for the biosensing application given in this work, but also for applications such as energy converting on fuel cells.

The optimal Pd-AuNPs (70% Pd, 30% Au) are used as tags, taking advantage of the bio-functionalities of gold present in the cluster, in an electrochemical immunosensor for the detection of hyaluronidase wound infection biomarker, using magnetic beads (MBs) platforms. The low matrix effects inherent to the use of MBs platforms allow us to discriminate between wound exudates with both sterile and infected ulcers without sample pre-treatment, meeting the clinical requirements. This novel electrocatalytic immunoassay has the advantage, over common methods for NP tags electrochemical detection, of the signal generation in the same neutral medium where the immunoassay takes place (10 mM PBS pH 7.4), avoiding the use of additional and hazardous reagents, bringing it closer to their use as point-of-care devices. This is of particular relevance in highly integrated systems such as lateral-flow assays, where our Pd-AuNPs have also potential interest, since their optical properties (violet color with maximum of absorbance at 530 nm) allows to postulate them as tags for dual electrochemical/optical detection.

Declaration of competing interest

The authors declare that they have no known competing financial interests or personal relationships that could have appeared to influence the work reported in this paper.

Acknowledgemnets

This work has been supported by the CTQ2017-86994-R and MCI-21-PID2020-115204RB-I00 projects from the Spanish Ministry of Economy and Competitiveness (MINECO) and the Spanish Ministry of Science and Innovation (MICINN) respectively, and the FC-GRUPIN-ID/2018/000166 project from the Asturias Regional Government. C. Toyos-Rodríguez thanks the MICINN for the award of a FPI Grant (PRE2018-084953). A. de la Escosura-Muñiz also acknowledges the MICINN for the "Ramón y Cajal" Research Fellow (RyC-2016-20299). The authors acknowledge the Chronic Ulcers Unit of the Hospital Universitario Central de Asturias (HUCA) and specially to Susana Valerdiz for providing the real samples used in this work.

References

Ahmadi, M., Ghoorchian, A., Dashtian, K., Kamalabadi, M., Madrakian, T., Afkhami, A., 2021. Talanta 225, 121974.
Ambrosi, A., Castañeda, M.T., Killard, A.J., Smyth, M.R., Alegret, S., Merkoçi, A., 2007. Anal. Chem. 79, 5232–5240.
Baptista-Pires, L., de la Escosura-Muñiz, A., Balsells, M., Zuaznabar-Gardona, J.C., Merkoçi, A., 2019. Electrochem. Commun. 98, 6–9.
Bayda, S., Adeel, M., Tuccinardi, T., Cordani, M., Rizzolio, F., 2020. Molecules 25, 112.
Brust, M., Walker, M., Bethell, D., Schiffrin, D.J., Whyman, R., 1994. J. Chem. Soc., Chem. Commun. 801–802, 0.
Campbell, C.T., 2004. Science 306, 234–235.
Cao, L., Cai, J., Deng, W., Tan, Y., Xie, Q., 2020. Anal. Chem. 92, 16267–16273.
Carneiro, P., Morais, S., Pereira, M.C., 2019. Nanomaterials 9, 1663.
Chen, D., Zhu, X., Tao, W., Kong, Y., Huag, Y., Zhang, Y., Liu, R., Jiang, L., Tang, Y., Yu, H., Hao, Q., Yang, X., Zou, H., Chen, J., Lu, Y., Zhang, H., Li, W., 2020. J. Contr. Release 324, 545–559.
Clinton, A., Carter, T., 2015. Lab. Med. 46, 277–284.
de la Escosura-Muñiz, A., Ambrosi, A., Merkoçi, A., 2008. TrAC Trends Anal. Chem. (Reference Ed.) 27, 568–584.
de la Escosura-Muñiz, A., Sánchez-Espinel, C., Díaz-Freitas, B., González-Fernández, A., Maltez-da Costa, M., Merkoçi, A., 2009. Anal. Chem. 81, 10268–10274.
de la Escosura-Muñiz, A., Merkoçi, A., 2010. Expert Opin. Med. Diagn. 4, 21–37.
de la Escosura-Muñiz, A., Parolo, C., Merkoçi, A., 2010a. Mater. Today 13, 24–34.
de la Escosura-Muñiz, A., Maltez-da Costa, M., Sánchez-Espinel, C., Díaz-Freitas, B., Fernández-Suarez, J., González-Fernández, Á., Merkoçi, A., 2010b. Biosens. Bioelectron. 26, 1710–1714.
de la Escosura-Muñiz, A., Plichta, Z., Horák, D., Merkoçi, A., 2015. Biosens. Bioelectron. 67, 162–169.
de la Escosura-Muñiz, A., Baptista-Pires, L., Serrano, L., Altet, L., Francino, O., Sánchez, A., Merkoçi, A., 2016. Small 12, 205–213.
de la Escosura-Muñiz, A., Ivanova, K., Tzanov, T., 2019. ACS Appl. Mater. Interfaces 11, 13140–13146.
Doria, G., Conde, J., Veigas, B., Giestas, L., Almeida, C., Assunção, M., Rosa, J., Baptista, P.V., 2012. Sensors 12, 1657–1687.
Gu, W., Yan, Y., Zhang, C., Xian, Y., 2016. ACS Appl. Mater. Interfaces 8, 11272–11279.
Han, A., Zenilman, J.M., Melendez, J.H., Shirtliff, M.E., Agostinho, A., James, G., Stewart, P.S., Mongodin, E.F., Rao, D., Rickard, A.H., Lazarus, G.S., 2011. Wound Repair Regen. 19, 532–541.
Han, G., Ceilley, R., 2017. Adv. Ther. 34, 599–610.
Han, J.-J., Li, N., Zhang, T.-Y., 2009. J. Power Sources 193, 885–889.
Hasmann, A., Wehrschuetz-Sigl, E., Kanzler, G., Gewessler, U., Hulla, E., Schneider, K.P., Binder, B., Schintler, M., Guebitz, G.M., 2011. Diagn. Microbiol. Infect. Dis. 71, 12–23.
Hassan, A.-R.H.A.-A., de la Escosura-Muñiz, A., Merkoçi, A., 2015. Biosens. Bioelectron. 67, 511–515.
Holzinger, M., Le Goff, A., Cosnier, S., 2014. Front. Chem. 2, 63.
Huizhi, K., Wang, L., O'Donoghue, M., Cao, Y.C., Tan, W., 2008. Nanoparticles for Biosensors 583–621 (Chapter 15).
Hynes, W.L., Walton, S.L., 2000. FEMS Microbiol. Lett. 183, 201–207.
Iglesias-Mayor, A., Amor-Gutiérrez, O., Costa-García, A., de la Escosura-Muñiz, A., 2019. Sensors 19, 5137.
Iglesias-Mayor, A., Amor-Gutiérrez, O., Novelli, A., Fernández-Sánchez, M.-T., Costa-García, A., de la Escosura-Muñiz, A., 2020. Anal. Chem. 92, 7209–7217.
Järbrink, K., Ni, G., Sönnergren, H., Schmidtchen, A., Pang, C., Bajpai, R., Car, J., 2016. Syst. Rev. 5, 152.
Kusunoki, K., Kudo, D., Hayashi, K., Chida, Y., Todoroki, N., Wadayama, T., 2021. ACS Catal. 11, 1554–1562.
Lara, S., Pérez-Potti, A., 2018. Biosensors 8, 104.
Li, Z., Chen, H., Zhuo, Z., Huang, D., Luo, F., Chen, L., Wang, J., Guo, L., Qiu, B., Lin, Z., 2018. Sensor. Actuator. B Chem. 275, 409–414.
Li, Z.-X., Zhang, J.-L., Wang, J., Luo, F., Qiu, B., Guo, L.-H., Lin, Z.-Y., 2021. J. Anal. Test. 5, 69–75.
Lim, D.-H., Wilcox, J., 2012. J. Phys. Chem. C 116, 3653–3660.
Liu, Q., Yan, X., Lai, Q., Su, X., 2019. Sensor. Actuator. B Chem. 282, 45–51.
Ma, R., Lin, G., Zhou, Y., Liu, Q., Zhang, T., Shan, G., Yang, M., Wang, J., 2019. Comput. Mater. 5, 78.
Maduraiveeran, G., 2021. Mater. Lett. 283, 128763.
Mahnic, A., Breznik, V., Bombek Ihan, M., Rupnik, M., 2021. Front. Med. 8, 607255.
Maltez-da Costa, M., de la Escosura-Muñiz, A., Nogués, C., Barrios, L., Ibáñez, E., Merkoçi, A., 2012. Small 8, 3605–3612.
Maltez-da Costa, M.M., la Escosura-Muñiz, A. de, Merkoçi, A., 2010. Electrochem. Commun. 12, 1501–1504.
Melendez, J.H., Frankel, Y.M., An, A.T., Williams, L., Price, L.B., Wang, N.-Y., Lazarus, G. S., Zenilman, J.M., 2010. Clin. Microbiol. Infect. 16, 1762–1769.
Mota, F.A.R., Pereira, S.A.P., Araújo, A.R.T.S., Passos, M.L.C., Saraiva, M.L.M.F.S., 2021. TrAC Trends Anal. Chem. (Reference Ed.) 143, 116405.
Nørskov, J.K., Rossmeisl, J., Logadottir, A., Lindqvist, L., Kitchin, J.R., Bligaard, T., Jónsson, H., 2004. J. Phys. Chem. B 108, 17886–17892.
Rahman, S.T., Rhee, K.Y., Park, S.-J., 2021. Nanotech. Rev. 10, 137–157.
Raj, P., Lee, S., Lee, T.Y., 2021. Materials 14, 1313.
Rivas, L., delaEscosura-Muñiz, A., Pons, J., Merkoçi, A., 2014. Electroanalysis 26, 1287–1294.
Rößner, L., Armbrüster, M., 2019. ACS Catal. 9, 2018–2062.
Schmidtchen, Helene Wolff, Carita H, A., 2001. Acta Derm. Venereol. 81, 406–409.
Serra, R., Grande, R., Butrico, L., Rossi, A., Settimio, U.F., Caroleo, B., Amato, B., Gallelli, L., de Franciscis, S., 2015. Ther 13, 605–613.
Sha, J., Paul, S., Dumeignil, F., Wojcieszak, R., 2019. RSC Adv. 9, 29888–29901.
Silva, N.H.C.S., Garrido-Pascual, P., Moreirinha, C., Almeida, A., Palomares, T., Alonso-Varona, A., Vilela, C., Freire, C.S.R., 2020. Biol. Macromol. 165, 1198–1210.
Singh, P., Buttry, D.A., 2012. J. Phys. Chem. C 116 (19), 10656–10663.
Spendelow, J.S., Wieckowski, A., 2007. Phys. Chem. Chem. Phys. 9, 2654.

Stern, R., Jedrzejas, M.J., 2006. Chem. Rev. 106, 818–839.
Tammeveski, L., Erikson, H., Sarapuu, A., Kozlova, J., Ritslaid, P., Sammelselg, V., Tammeveski, K., 2012. Electrochem. Commun. 20, 15–18.
Tang, J., Tang, D., 2015. Microchim. Acta 182, 2077–2089.
Tian, X., Lu, X.F., Xia, B.Y., Lou, X.W., David, 2020. Joule 4, 45–68.
Toshima, N., Kanemaru, M., Shiraishi, Y., Koga, Y., 2005. J. Phys. Chem. B 109, 16326–16331.
Toyos-Rodríguez, C., García-Alonso, F.J., de la Escosura-Muñiz, A., 2020. Sensors 20, 4748.
Verbanic, S., Shen, Y., Lee, J., Deacon, J.M., Chen, I.A., 2020. npj Biofilms Microbiomes 6, 21.
Wang, A., Liu, X.Y., Mou, C.-Y., Zhang, T., 2013. J. Catal. 308, 258–271.
Wang, H.-Y., Weng, C.-C., Yuan, Z.-Y., 2021. J. Energy Chem. 56, 470–485.
Wang, Q., Fu, W., Ma, R., Lu, Q., Liu, Z., Yao, J., Liu, Q., Zhang, X., Zhao, H., 2022. Dyes Pigm 197, 109844.
Wang, X., Choi, S.-I., Roling, L.T., Luo, M., Ma, C., Zhang, L., Chi, M., Liu, J., Xie, Z., Herron, J.A., Mavrikakis, M., Xia, Y., 2015a. Nat. Commun. 6, 7594.
Wang, X., Vara, M., Luo, M., Huang, H., Ruditskiy, A., Park, J., Bao, S., Liu, J., Howe, J., Chi, M., Xie, Z., Xia, Y., 2015b. J. Am. Chem. Soc. 137, 15036–15042.
Welch, C.M., Compton, R.G., 2006. Anal. Bioanal. Chem. 384, 601–619.
Wittenberg, N.J., Haynes, C.L., 2009. WIREs Nanomed. Nanobiotechnol. 1, 237–254.
Wu, Z.-P., Caracciolo, D.T., Maswadeh, Y., Wen, J., Kong, Z., Shan, S., Vargas, J.A., Yan, S., Hopkins, E., Park, K., Sharma, A., Ren, Y., Petkov, V., Wang, L., Zhong, C.-J., 2021. Nat. Commun. 12, 859.
Zhang, H., Watanabe, T., Okumura, M., Haruta, M., Toshima, N., 2012. Nat. Mater. 11, 49–52.
Zhao, D., Xu, B.-Q., 2006. Angew. Chem. Int. Ed. 45, 4955–4959.
Zhou, X., Willems, R.J.L., Friedrich, A.W., Rossen, J.W.A., Bathoorn, E., 2020. Antimicrob. Resist. Infect. Control 9, 130.